S. Zykov, *Biophysics* **25**, 906 (1980).
13. D. Barkley, *Physica D* **49**, 61 (1991).
14. The functions f and g are defined as $f(u, v) = (1/\epsilon)u(1 - u)[u - (v + b)/a]$ and $g(u, v) = u - v$. The parameter values $a = 0.9$, $b = 0.05$, and $\epsilon = 0.02$ were chosen to model an excitable system. The equations were integrated on a grid of 480 points by 480 points (grid spacing $\Delta x = 1.3$, time step $\Delta t = 0.085$) with the Laplacian operator ∇^2 approximated by a standard nine-point formula. (The same optimal path was found in a higher resolution calculation with grid spacing $\Delta x = 0.65$ and time step $\Delta t = 0.011$.) We were able to realize different complex labyrinths by digitizing corresponding line drawings and modeling the borders and obstacles as regions with constant, steady-state values of u and v. These boundary conditions correspond to "sink" boundaries and reflect the experimental system, where all edges of the membrane were in contact with silicone oil.
15. W. H. Matthews, *Mazes and Labyrinths* (Longmans, London, 1922).
16. Á. Tóth, V. Gáspár, K. Showalter, *J. Phys. Chem.* **98**, 522 (1994).
17. E. R. Kandel, J. H. Schwartz, T. M. Jessell, *Principles of Neural Science* (Elsevier, New York, ed. 3, 1991).
18. M. D. Graham *et al.*, *Science* **264**, 80 (1994).
19. This research was supported by the National Science Foundation (grant CHE-9222616). We acknowledge the donors of the Petroleum Research Fund, administered by the American Chemical Society, for partial support of this research.

26 August 1994; accepted 10 November 1994

Electrochemical Detection of Single Molecules

Fu-Ren F. Fan and Allen J. Bard*

The electrochemical behavior of a single molecule can be observed by trapping a small volume of a dilute solution of the electroactive species between an ultramicroelectrode tip with a diameter of ~15 nanometers and a conductive substrate. A scanning electrochemical microscope was used to adjust the tip-substrate distance (~10 nanometers), and the oxidation of [(trimethylammonio)methyl] ferrocene (Cp_2FeTMA^+) to Cp_2FeTMA^{2+} was carried out. The response was stochastic, and anodic current peaks were observed as the molecule moved into and out of the electrode-substrate gap. Similar experiments were performed with a solution containing two redox species, ferrocene carboxylate (Cp_2FeCOO^-) and $Os(bpy)_3^{2+}$ (bpy is 2,2′-bipyridyl).

A number of techniques have been used in recent years to detect single molecules or ions in different environments. These include the detection of ions that are confined in vacuum in electromagnetic traps (*1*), single-molecule spectroscopy of molecules in solid matrices (*2*), and the detection of molecules on surfaces with high spatial resolution by near-field scanning optical microscopy (*3*). These techniques are based largely on observation of the fluorescent emission from the molecule during repeated photonic excitation events and provide information about energy levels and the environment of the molecule. We report single-molecule detection (SMD) for an electroactive molecule in solution as it repeatedly undergoes electron-transfer reactions at an electrode held at a small distance from a counterelectrode in a scanning electrochemical microscope (SECM) (*4*, *5*).

The principle of this experiment is illustrated in Fig. 1. To achieve SMD in the SECM, a small tip electrode of nanometer dimensions and with a geometry that provides confinement of the molecule near the active tip area is held near (~10 nm) a conductive substrate. The solution concentration is adjusted so that, on average, only a single molecule will reside in the volume defined by the tip area and tip-substrate spacing d. Consider a tip of radius $a = 5$ nm held at $d = 10$ nm. For a 2 mM solution of an electroactive species, it is probable that only one molecule will be present in the $\sim 10^{-18}$ cm^3 volume beneath the tip (*5*). The time required for the molecule to transit between tip and substrate is of the order of $d^2/2D$, where D is the diffusion coefficient of the molecule. Thus, a molecule with $D = 5 \times 10^{-6}$ cm^2/s will transit the gap in about 100 ns or undergo ~10^7 round trips between tip and substrate per second. If an electron-transfer event occurs at each collision with the tip, a current of the order of 1 pA will flow. In this case, SMD depends on the 10^7 amplification factor provided by the positive feedback of the SECM. The molecule is confined to the space below the tip because the conductive tip is slightly recessed below the large insulating sheath that surrounds it, as shown in Fig. 1. Further axial confinement of a charged species might be afforded by the electric field in the gap.

For the initial test of SMD by SECM we chose [(trimethylammonio)methyl] ferrocene (Cp_2FeTMA^+) as the electroactive molecule, because both this species and its oxidized product are stable in aqueous media and undergo rapid heterogeneous electron-transfer reactions at electrodes in a convenient range of potentials. Solutions contained 2 mM Cp_2FeTMA^+ with $NaNO_3$ as the supporting electrolyte. In all of the experiments, an indium-tin oxide (ITO, Delta Technologies, Stillwater, New York) electrode was used as substrate. The tip was fabricated from an electrochemically sharpened 125-μm Pt-Ir (80%-20%) wire coated with Apiezon wax or polyethylene glue. We exposed the end by placing the tip in a scanning tunneling microscope (STM) and allowed it to approach the ITO substrate until a set-point current (0.5 nA) began to flow. By constructing the tip in this manner, we ensured that the tip and its insulating sheath would approach the ITO surface perpendicularly without alignment difficulties. Details of the fabrication of these tips and their characterization are given elsewhere (*5*–*7*). The instrument used in these studies has been described in (*8*, *9*) and is capable of both STM and SECM measurements with a vertical (z direction) resolution of better than 1 Å and a current sensitivity as low as 50 fA when the proper filter is used. The electrochemical cell contained a Pt counterelectrode and either a saturated calomel electrode (SCE) or a Pt quasi-reference electrode.

The correct tip geometry is essential for the successful trapping of a molecule. Information about the exposed area of the tip and the shapes of the tip and insulating sheath can be obtained from electrochemical measurements, that is, from determination of the tip current i_T as a function of d as the tip is moved toward the substrate in an SECM (*7*). All of the tip currents reported were corrected for the background current in the blank solution, that is, a solution containing only supporting electrolyte, at large d. A typical approach curve of this type taken with a solution of 2 mM Cp_2FeTMA^+ and 2.0 M $NaNO_3$, with the tip held at 0.55 V versus SCE where Cp_2FeTMA^+ oxidation is diffusion-controlled, is shown in Fig. 2. The ITO substrate was biased at −0.3 V versus SCE, so that Cp_2FeTMA^{2+} generated at the tip was rapidly reduced back to Cp_2FeTMA^+ at the ITO surface. The exposed radius a can be found (*5*) from the steady-state current $i_{T,\infty}$, when the tip is assumed to be a disk-shaped

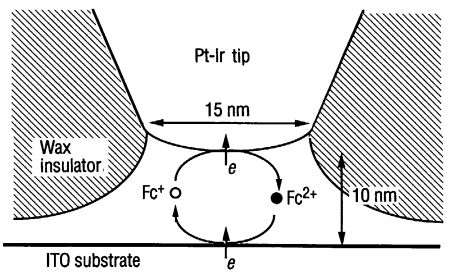

Fig. 1. Idealized schematic illustration of the tip geometry and the tip-substrate configuration used.

Department of Chemistry and Biochemistry, University of Texas, Austin, TX 78712, USA.

*To whom correspondence should be addressed.

electrode far from the substrate, with the equation

$$i_{T,\infty} = 4nFDCa \quad (1)$$

where n is the number of electrons involved in the redox reaction (1 for Cp_2FeTMA^+), F is the Faraday constant, the diffusion coefficient D is 5.0×10^{-6} cm^2/s, and C is the concentration of Cp_2FeTMA^+ (2 mM). This calculation yields a disk diameter of 15 nm.

The SECM positive-feedback process starts to become significant when the tip approaches a conductive substrate to within a few tip diameters and i_T increases. However, with tips constructed as described above, the current then decreases as the tip comes even closer (point A in Fig. 2) before showing a large increase (starting at point E). Although this current decrease might be attributed to heterogeneous kinetic effects on the electron-transfer reactions (*10*), this behavior was found at even more extreme tip and ITO potentials and with other redox couples with tips of this type. We thus believe that this region of current decrease represents blocking of mass transfer from the bulk solution into the tip-substrate gap by the insulating sheath (radius $\geq 25a$) surrounding the exposed tip. For a perfectly planar tip and insulating sheath approaching a parallel insulating substrate, a transition occurs from hemispherical diffusion when the tip is far from the substrate to planar diffusion when the tip is near the substrate, because the large insulating sheath restricts radial diffusion. The transition from spherical to linear diffusion causes a decrease in the tip current of the order of $a/2d$, so that when $d = a$, $i_T = 0.5i_{T,\infty}$. With a conductive substrate, the positive feedback compensates for this blocking effect and causes a net increase in current. However, we believe that, in the tips fabricated as described above, the conductive electrode portion is slightly recessed into the insulating sheath, so that, at small distances, solution is trapped in a small pocket near the electrode as shown in Fig. 1. Upon further decrease in d, the insulating sheath is compressed and both SECM feedback and the onset of tunneling cause the current to increase again (Fig. 2, point E).

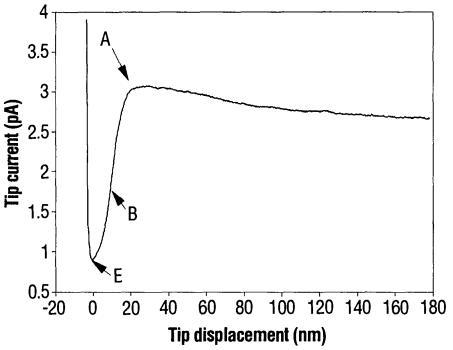

Fig. 2. Dependence of tip current on relative tip displacement over a conductive ITO substrate in a solution containing 2 mM Cp_2FeTMA^+ and 2.0 M $NaNO_3$. The ITO substrate was biased at −0.3 V versus SCE and the tip was biased at 0.55 V, where the redox reactions on both electrodes were diffusion-controlled. The tip moved to the substrate surface at a rate of 30 Å/s. The data were 300 points averaged at each location. The significance of points A, B, and E is discussed in the text. See also Fig. 4.

The blocking effect of the insulating sheath is also reflected in the tip double-layer charging process. We observed a series of current transient (charging) curves at several d values (2 to 19 nm) for a tip with a diameter of ~20 nm in a solution containing only 1.0 M $NaNO_3$ by stepping the tip potential from 0.15 to 0.6 V versus SCE (Fig. 3). From an analysis of the exponential decay of curve 1 (d = 19 nm), an uncompensated resistance of ~0.2 gigohms and an equivalent series capacitance of about 4 pF were found. This resistance is considerably larger than that calculated for a sphere of this radius, suggesting considerable blockage by the surrounding sheath. The equivalent series capacitance is also much larger than the double-layer capacitance of the tip and is governed by the input capacitance (~3 pF) of the preamplifier of the SECM. When we decreased d, the capacitance essentially retained its value while the uncompensated resistance increased to ~5 gigohms at d = 2 nm (curve 5 in Fig. 3) as the solution channel to the tip was further compressed.

Cyclic voltammograms (i_T versus tip potential E_T), which can be taken by stopping at different points on the approach curve (Fig. 4), show the oxidation of Cp_2FeTMA^+ at a scan rate of 10 mV/s at d values of about 30, 20, and 10 nm. The curve taken at point A in Fig. 2 (curve 1 of Fig. 4A) shows the expected steady-state voltammetric shape with a flat plateau current region that retraces upon scan reversal. This behavior demonstrates that the current decrease observed in the approach curve represents the steady-state current and not a transient. As d is decreased, the voltammetric curve retains its shape, but the current throughout is smaller (curve 2 of Fig. 4A). When $d \leq 10$ nm (curve 3), the current is characterized by large fluctuations. To show these current fluctuations in the diffusion-controlled region more clearly, we also plotted i_T and E_T for curve 3 as functions of time in Fig. 4B.

Similar fluctuations were observed when the electrode was moved close to the substrate, held at a potential in the plateau region (for example, 0.55 V versus SCE), and i_T was measured as a function of time (Fig. 5, curve A). Although the signal was noisy, the current showed clear peaks of 0.7 and 1.4 pA as well as periods of essentially zero average current. We believe that these represent current responses when one or two Cp_2FeTMA^+ molecules are trapped in the 10-nm gap between the tip and substrate and drift into or out of the tip region.

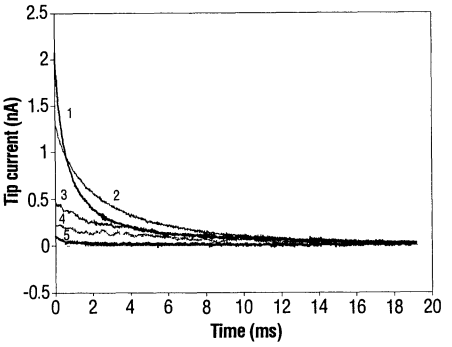

Fig. 3. The charging curves at a tip with an estimated diameter of ~20 nm in a solution containing only 1 M $NaNO_3$. The tip potential was stepped from 0.15 to 0.6 V versus SCE at d = 19 nm (curve 1), 12 nm (curve 2), 9 nm (curve 3), 5 nm (curve 4), and 2 nm (curve 5). The data sampling rate was 20 μs per point.

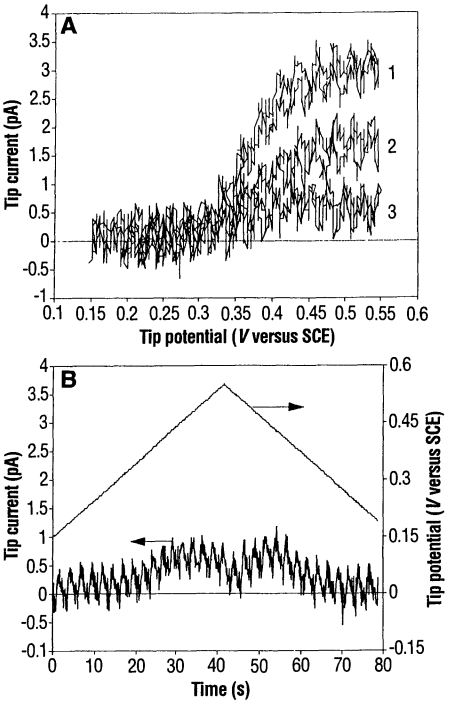

Fig. 4. (**A**) Series of cyclic voltammograms taken at different tip-substrate separations in a solution containing 2 mM Cp_2FeTMA^+ and 2.0 M $NaNO_3$. The substrate potential was −0.3 V versus SCE, and the scan rate of the tip potential was 10 mV/s. Curve 1 was taken at a d of about point A in Fig. 2; curve 2 was taken at 15 nm from point E; curve 3 was taken at about 5 nm away from the surface relative to point E, where the fluctuation in i_T occurred. In all cases, we take point E in Fig. 2 as the reference point. (**B**) Plots of i_T and E_T from curve 3 in (A) as functions of time.

As a control experiment, curve B in Fig. 5 was taken when the tip was farther from the substrate; it shows a constant average current over a 300-s measurement period.

To show that the fluctuations seen at small d do not represent thermal drift of the tip (bringing it into and out of tunneling distance), we studied the behavior with the tip closer to the substrate in a solution containing only supporting electrolyte. In the absence of Cp_2FeTMA^+, the average current was essentially zero until tunneling distances were attained. At that point (curve C in Fig. 5), the initial current was higher than that in curve A, with very large short-term current spikes that probably represent thermal fluctuations and vibrations. These are very different from the smoother broad peaks seen with electroactive species when the tip is located at slightly larger distances in curve A.

Without a better picture of the details of the tip and insulator structure, it is difficult to explain the rather slow fluctuations in current (on the order of tens of seconds) and the shape of the responses. One possibility is that the insulator is cracked during the tip exposure part of the fabrication, resulting in tiny channels connected to small reservoirs or to the bulk solution that are not in direct contact with the tip. When the molecule passes into these reservoirs, no current is seen until it traverses the channel back into the tip volume. There is also some drift in the tip-substrate spacing, for example, because of temperature fluctuations and relaxation of the z-piezo element, which affects the tip current.

In another independent experiment to show SMD in the SECM, a new solution and a new tip were used. The current was monitored with time at different potentials with the tip held at ~10 nm from the substrate (at −0.3 V versus SCE) where the "peaking behavior" is seen (Fig. 6). As in the earlier experiments, when the tip potential was 0.55 V, peaks were observed. When the tip potential was switched to 0.0 V, that is, to the foot of the voltammetric wave where no oxidation of Cp_2FeTMA^+ occurs, the current immediately dropped to the background level and remained there for ~150 s. Then the tip potential was again switched to 0.55 V, resulting in an immediate capacitive current transient and then fluctuating oxidation current, as before. Switching to a more positive potential in the diffusion-limited region (0.70 V) produced essentially the same type of peaks as those at 0.55 V, as expected. However, when the potential was again switched to the foot of the voltammetric wave, 0.15 V, only background current was observed. In the experiments in which only background currents were seen, the bias between tip and substrate was either 0.3 or 0.45 V. The absence of currents in this region strongly suggests that the observed peaks cannot be attributed to tunneling current fluctuations.

In another independent experiment to show that the observed response is associated with the redox molecules, we used a new tip and a solution of two redox couples at different concentrations. We selected Cp_2FeCOO^- (2 mM) and $Os(bpy)_3^{2+}$ (bpy is 2,2′-bipyridyl) (4 mM) as the electroactive species. As shown in Fig. 7, the tip current was monitored with time at different potentials with the tip held at a position above the substrate where a substantial current fluctuation was observed. As in the case of Cp_2FeTMA^+, when the tip potential was 0.5 V, where the diffusion-controlled current for the oxidation of Cp_2FeCOO^- was observed, peaks were observed. When the tip potential was switched to 0.8 V, that is, to the current plateau region of the voltammetric wave for the oxidation of $Os(bpy)_3^{2+}$, an immediate capacitive current transient and then higher oxidation current peaks were observed. The increased current heights are consistent with an increased total concentration of redox-active species [Cp_2FeCOO^- and $Os(bpy)_3^{2+}$] and cannot be attributed to tunneling current fluctuations that are exponentially dependent on the potential. The absence of significant current fluctuations in the time domain of ~180 to 230 s, during which the tip potential was switched between 0.0 and 0.5 V, also strongly suggests that the observed current peaks in the other time domains are not due to potential-dependent tunneling current fluctuations.

We assert that the data in Figs. 5, 6, and 7 are evidence for SMD in a zeptoliter (zepto = 10^{-18}) volume below the tip, with the electrochemistry at the single-molecule level occurring in a stochastic process. Confinement of the molecule to this volume is largely attributable to the concave shape of the tip that forms naturally during fabrication. A scanning electron microscope (SEM) image of the tip, although incapable of resolving the conductive tip itself, shows a depression in the surrounding insulator with a radius of ~0.4 μm. The maximum peak currents are also consistent with SMD, because the expected current for a single-molecule event in this geometry, of the order of De/d^2 (where e is the electronic charge), is 0.8 pA. Moreover, the essentially "quantized" peak current values in Fig. 5, curve A, suggest differentiation between trapping of one or two molecules. The electric field in the gap may also influence the observed behavior. In experiments with the SECM, we have found (*11*) large changes in tip current at very small supporting electrolyte concentrations, suggesting migration

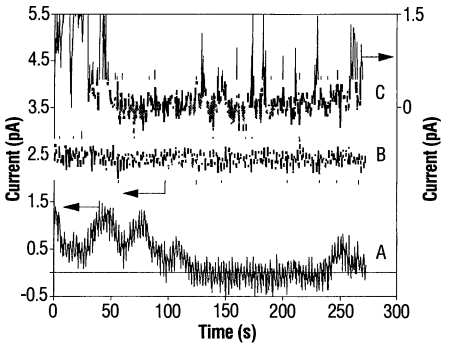

Fig. 5. Time evolution of the tip current observed at a tip potential of 0.55 V and a substrate potential of −0.3 V versus SCE. The initial tip current in curves A and C was set by allowing the tip to approach the substrate until $i_T \approx 1.5$ pA. Curve A: tip-substrate separation of ~10 nm in a solution containing 2 mM Cp_2FeTMA^+ and 2.0 M $NaNO_3$ (left current scale). Curve B: with the tip far from the substrate in same solution as in curve A (left current scale). Curve C: tip-substrate separation within tunneling range in a solution containing only 2.0 M $NaNO_3$ (right current scale). The data sampling rate was 0.4 s per point.

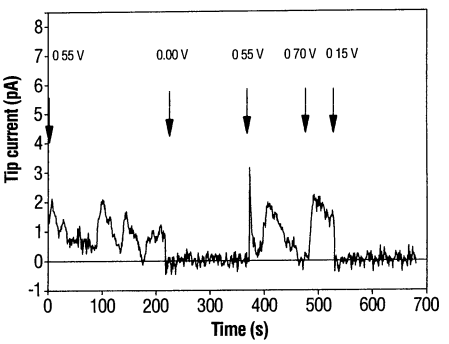

Fig. 6. Time evolution of tip current with a substrate potential of −0.3 V versus SCE at various tip potentials E_T (indicated above the arrows). We set the initial tip current at ~1.5 pA by adjusting d. The solution contained 2 mM Cp_2FeTMA^+ and 2.0 M $NaNO_3$. The data sampling rate was 1 s per point.

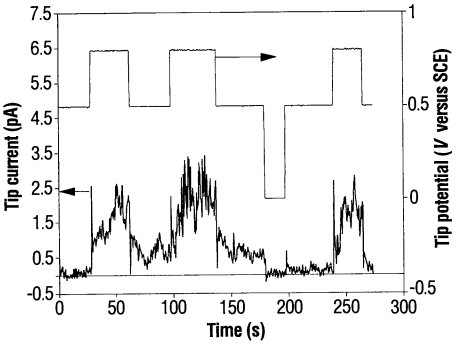

Fig. 7. Time evolution of tip current with a substrate potential of −0.3 V versus SCE at various tip potentials E_T. We set the initial tip current at ~0.5 pA by adjusting d. The solution contained 2 mM Cp_2FeCOO^-, 4 mM $Os(bpy)_3^{2+}$, and 0.5 M $NaNO_3$. The data sampling rate was 0.4 s per point.

and diffuse double-layer structure effects (*12*). Electrochemical experiments at the single-molecule level can provide information complementary to spectroscopic experiments and might allow one to examine kinetic models at a level at which continuous approximations are not appropriate.

REFERENCES AND NOTES

1. See, for example, W. M. Itano, J. C. Bergquist, D. J. Wineland, *Science* **237**, 612 (1987), and references therein; F. Diedrich *et al.*, *IEEE J. Quantum Electron.* **24**, 1314 (1988).
2. W. E. Moerner, *Science* **265**, 46 (1994).
3. E. Betzig and R. J. Chichester, *ibid.* **262**, 1422 (1993); W. P. Ambrose, P. M. Goodwin, J. C. Martin, R. A. Keller, *Phys. Rev. Lett.* **72**, 160 (1994).
4. A. J. Bard, F.-R. F. Fan, J. Kwak, O. Lev, *Anal. Chem.* **61**, 132 (1989).
5. A. J. Bard, F.-R. F. Fan, M. V. Mirkin, in *Electroanalytical Chemistry*, A. J. Bard, Ed. (Dekker, New York, 1994), vol. 18, pp. 243–373.
6. L. A. Nagahara, T. Thundat, S. M. Lindsay, *Rev. Sci. Instrum.* **60**, 3128 (1989).
7. M. V. Mirkin, F.-R. F. Fan, A. J. Bard, *J. Electroanal. Chem.* **328**, 47 (1992).
8. F.-R. F. Fan, M. V. Mirkin, A. J. Bard, *J. Phys. Chem.* **98**, 1475 (1994).
9. F.-R. F. Fan and A. J. Bard, *J. Electrochem. Soc.* **136**, 3216 (1989).
10. M. V. Mirkin and A. J. Bard, *J. Electroanal. Chem.* **323**, 1 (1992).
11. F.-R. F. Fan and A. J. Bard, unpublished data.
12. C. P. Smith and H. S. White, *Anal. Chem.* **65**, 3343 (1993).

13. Supported by the Robert A. Welch Foundation and the National Science Foundation. We thank J. Armstrong for SEM images of the tip.

30 August 1994; accepted 12 December 1994

High Sex Ratios in China's Future

Shripad Tuljapurkar,* Nan Li, Marcus W. Feldman

In China in recent years, male live births have exceeded those of females by amounts far greater than those that occur naturally in human populations, a trend with significant demographic consequences. The resulting imbalance in the first-marriage market is estimated to be about 1 million males per year after 2010. These "excess" males were not easily accommodated in models with substantial changes in first-marriage patterns. The current sex ratio at birth has little effect on a couple's probability of having at least one son, so future increases in the sex ratio may well occur, especially given increasing access to sex-selective abortion.

Among the reasons that China fascinates demographers are the recent rapid fall of its total fertility rate (*1*) and the remarkable rise in the reported sex ratio at birth (SRB). The SRB is the number of live male births for every hundred live female births in a reference period, usually a year, and historically the human SRB is near 105, changing little with parity (the number of children a mother has borne) (*2*). In China, the SRB for all births rose to 113.8 in 1990, and the SRB for higher parities was even higher (*3*, *4*). This imbalance of the sexes implies many millions of "missing" females (*5*). Some of these are unreported births, but a substantial number are missing because of high early female mortality or selective abortion (*6*–*8*). A pattern of declining fertility and high male bias in sex ratio at birth is also observed in countries such as India, Bangladesh, and South Korea (*9*).

We examine three demographic consequences of the sharp rise in China's SRB. First, the timing and size of the coming imbalance in the first-marriage market in China. Second, the effect of today's high SRB on the probability that an individual couple will have at least one son; presumably this is what couples with a strong son-preference aim to increase. Third, the effect of SRB on the "no-son dependency ratio" (NSDR), which measures the social "burden" presented by elderly people who have no son.

The prospects of marriage depend on many factors; we focus on the supply of potential mates, which depends on the SRB, marriage patterns, and population age structure. We measure the relative size of potential mating pools by a sex ratio R_F of potential first-marriage partners, computed as the ratio of male numbers weighted by age-specific first-marriage frequencies for males to female numbers weighted by the corresponding frequencies for females (*10*).

China's pattern of nearly universal marriage makes R_F particularly apropos (*1*, *4*). We projected China's population, starting with the 1990 census population holding fertility, mortality, and first-marriage frequencies constant at 1990 levels (*4*). In the projection, population vital rates are used to construct matrices that project births to females and the mortality of successive cohorts (*11*). Changes in mortality at late ages, or equal changes in mortality for both sexes at younger ages, would not qualitatively alter the conclusions. Fertility change in China depends strongly on government policy, which is not expected to change soon (*12*, *13*); the assumption of a different but constant fertility would not qualitatively change our results. Our projection uses parity-specific values of the SRB held constant at the 1990 level, a conservative assumption judging by recent trends (*3*, *6*–*8*). Even if the SRB were to fall, the phenomena we describe below are unavoidable in the medium term.

The ratio R_F is projected to be unbalanced through 2050 (Fig. 1). It rises to a peak over the next decade and declines rapidly by 2005, after which it rises towards a high level by 2050. The first peak is driven by the recent decline in fertility: Men marrying in a particular year come from earlier and larger birth cohorts than their younger partners. When fertility is constant for some years, this imbalance disappears. Beyond about 2005, however, marriage markets will be dominated by cohorts that had historically high sex ratios at birth. Starting about 2010, the recent high SRB will cause the marriage market ratios to go out of balance. If the upward trend in the SRB continues, the imbalance will be greater than shown in Fig. 1. For first marriages, which traditionally involve about 96% of each cohort (*1*, *4*), we find an imbalance in R_F of over 8% of males by 2020. This translates into about 1 million excess males per year in the market for first marriages.

What will happen to this "excess" of unmarried males? To marry, they will have to find mates outside the traditional cultural patterns that are summarized by the first-marriage frequencies. We explored the effect of two alternative changes (Fig. 2) in these patterns. In one, male marriage is delayed by 2 years at every age; in the other, age preferences for males and females are greatly relaxed by an increase in the variance in the age pattern of male and female marriage frequencies by a factor of 4. As shown in Fig. 3, neither change greatly alters the projected imbalance in R_F after 2010. Furthermore, historical evidence suggests that such large shifts in marriage patterns may face substantial social, economic, and cultural obstacles (*14*). The imbalance in the marriage market in China is the opposite of that found in the highly industrialized countries, where higher female life expectancy generates an "excess" of females [3 to 5% overall and more in some subgroups (*15*, *16*)].

The strong preference for sons in China

S. Tuljapurkar and M. W. Feldman, Morrison Institute for Population and Resource Studies, Department of Biological Sciences, Stanford University, Stanford, CA 94305, USA.

N. Li, Morrison Institute for Population and Resource Studies, Department of Biological Sciences, Stanford University, Stanford, CA 94305, USA, and Population Research Institute, Xi'an Jiaotong University, Xi'an, Shaanxi 710049, China.

*To whom correspondence should be addressed.